



Simulations of moving effect of coastal vegetation on tsunami damping

Ching-Piao Tsai¹, Ying-Chi Chen¹, Tri Octaviani Sihombing², and Chang Lin¹

¹Department of Civil Engineering, National Chung Hsing University, Taichung 402, Taiwan

²Department of Civil Engineering, Maranatha Christian University, Bandung, West Java 40164, Indonesia

Correspondence to: Ching-Piao Tsai (cptsai@nchu.edu.tw)

Received: 1 November 2016 – Discussion started: 23 December 2016

Accepted: 7 April 2017 – Published: 16 May 2017

Abstract. A coupled wave–vegetation simulation is presented for the moving effect of the coastal vegetation on tsunami wave height damping. The problem is idealized by solitary wave propagation on a group of emergent cylinders. The numerical model is based on general Reynolds-averaged Navier–Stokes equations with renormalization group turbulent closure model by using volume of fluid technique. The general moving object (GMO) model developed in computational fluid dynamics (CFD) code Flow-3D is applied to simulate the coupled motion of vegetation with wave dynamically. The damping of wave height and the turbulent kinetic energy along moving and stationary cylinders are discussed. The simulated results show that the damping of wave height and the turbulent kinetic energy by the moving cylinders are clearly less than by the stationary cylinders. The result implies that the wave decay by the coastal vegetation may be overestimated if the vegetation was represented as stationary state.

1 Introduction

A huge tsunami in Southeast Asia caused catastrophic damage and claimed more than 200 000 people in December 2004. Cochard et al. (2008) pointed out that this event has stimulated a debate about the role coastal ecosystems, such as mangrove forests and coral reefs, played in protecting low-lying coastal area. For example, Baird (2006) questioned the effectiveness of the coastal forests or reefs on the reduction of the damage caused by the tsunami. However, Danielsen et al. (2005) reported that areas with coastal tree vegetation

were markedly less damaged than areas without. Iverson and Prasad (2007) also indicated that developed areas were far more likely to be damaged than forested zones. Several studies (Hiraishi and Harada, 2003; Harada and Kawata, 2004; Teh et al., 2009) have shown that tsunami wave heights, velocities, and energies were significantly reduced as the wave propagates through mangrove forests. Nevertheless, Wolanski (2006) has noted that mangroves probably cannot protect the coast against a tsunami wave greater than a threshold level based on some evidence from observations of the Indian Ocean tsunami. Based on the field observations, Shuto (1987) and Yanagisawa et al. (2009) found that single trees or even entire forests could be destroyed through tilting, uprooting, bending, or trunk breaking by tsunami. Because tsunamis remain a threat to lives and property along the most coasts of the world, it remains important for estimating the effectiveness of the coastal vegetation on the tsunami impact.

Many numerical and experimental approaches have been developed in recent years to help understand the tsunami wave interactions with coastal vegetation. Coastal tree vegetation was idealized by a group of rigid cylinders in most investigations. Huang et al. (2011) performed both experiments and a numerical model by considering solitary wave propagation on emergent rigid cylinders and found that dense cylinders may reduce the wave transmission because of the increased wave energy dissipation into turbulence in cylinders. By using both direct numerical simulation and a macroscopic approach, Maza et al. (2015) simulated the interaction of solitary waves with emergent rigid cylinders based on the arrangement of laboratory experiments of Huang et al. (2011). Previous approaches (e.g. Anderson et al., 2011;

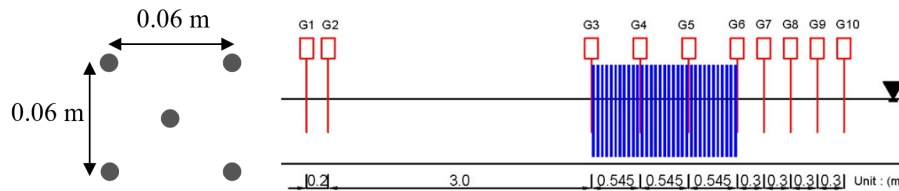


Figure 1. Cylinder cell arrangement (left), field length (right), and locations of wave probes for the computations.

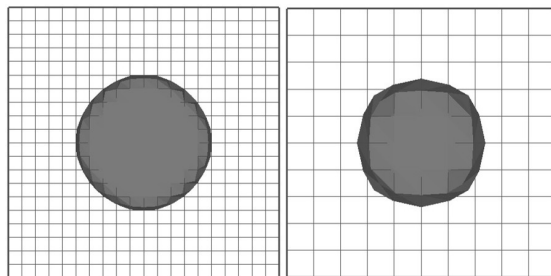


Figure 2. FAVOR technique geometry of cylinders and constructed computational rectangular grid with $0.001 \text{ m} \times 0.001 \text{ m}$ (left) and $0.002 \text{ m} \times 0.002 \text{ m}$ (right).

Huang et al., 2011; Maza et al., 2015; Wu et al., 2016) assumed that the idealized mangrove vegetation is stationary and neglected the plant motion with the wave.

Several works have investigated the hydraulic resistance of coastal vegetation involving the flexible effect of plants. Zhang et al. (2015) pointed out that the prop roots under tidal hydrodynamic loadings in a mangrove environment can be regarded as fairly rigid on account of a large Young modulus. However, Augustin et al. (2009) indicated that motion of the flexible elements is an important factor on wave attenuation based on flume tests considering both stiff and flexible parameterized tree models under wave action. Husrin (2013) found that the trunk of a mangrove, with its strength properties, may behave as a stiff or flexible structure which also governs its relative contribution to the total energy dissipation under tsunami and storm wave action. Coastal pines, which are typical of coastal forest vegetation, have longer trunk than mangroves; Husrin and Oumeraci (2013) indicated that they are more deflected when subject to similar flow velocity compared to mangroves. Husrin et al. (2012) and Strusińska et al. (2013, 2014) examined the tsunami attenuation by coastal vegetation under laboratory conditions for mature mangroves using parameterized trees, including flexible tree models. Maza et al. (2013) presented a new numerical model for the interaction of waves and flexible moving vegetation which couples the flow and the plant motion by considering the plant deformation using RANS equation with $k - \varepsilon$ turbulent model.

Some mangrove roots and branches at the growing stage are hanging from the canopy to the flow; this causes the prop roots to oscillate in the water. This study presents a nu-

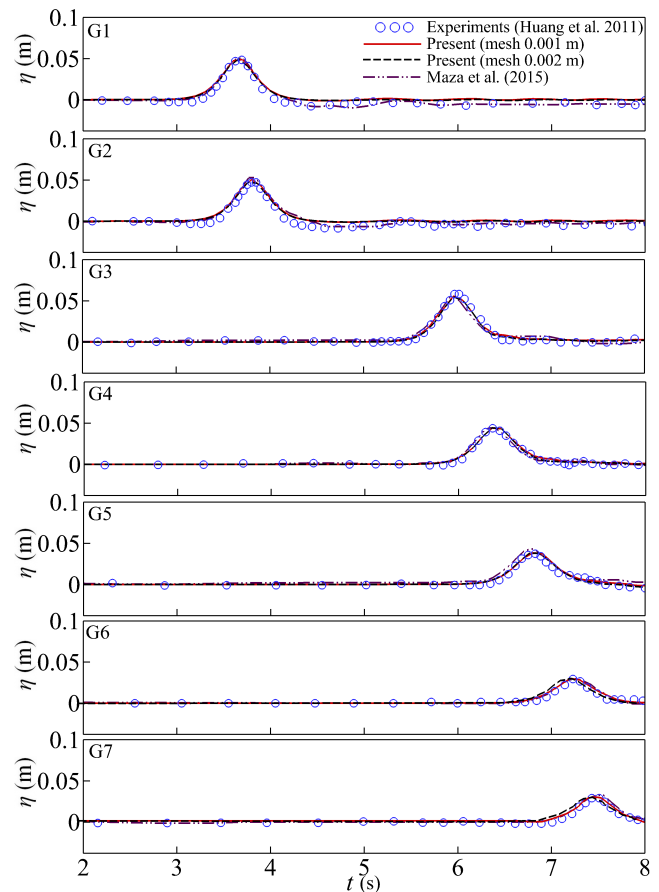


Figure 3. Comparison of free-surface evolution between numerical and experimental using field length of 1.635 m and $H_i = 0.05 \text{ m}$.

merical simulation that consider vegetation motion coupled with tsunami waves to investigate the wave-damping performance. We model the motion of the vegetation by attaching rigid cylinders to torsional connectors under wave action, which is similar to the experimental work of Kazemi et al. (2015). This is also a simplified way to represent some movements of mangroves induced by sediment scour, tilting, or uprooting states. A direct numerical model based on computational fluid dynamics (CFD) is presented in this paper for simulating the wave-damping characteristics by both stationary and moving vegetation.

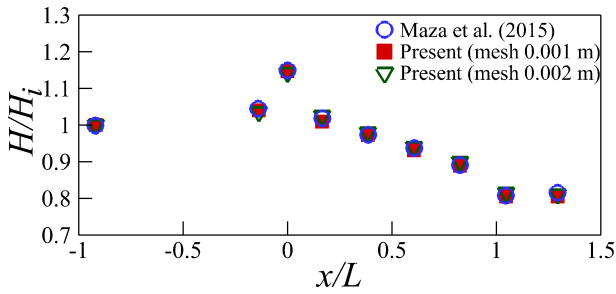


Figure 4. Comparison between the numerical results using the field length of 0.545 m and $H_i = 0.05$ m.

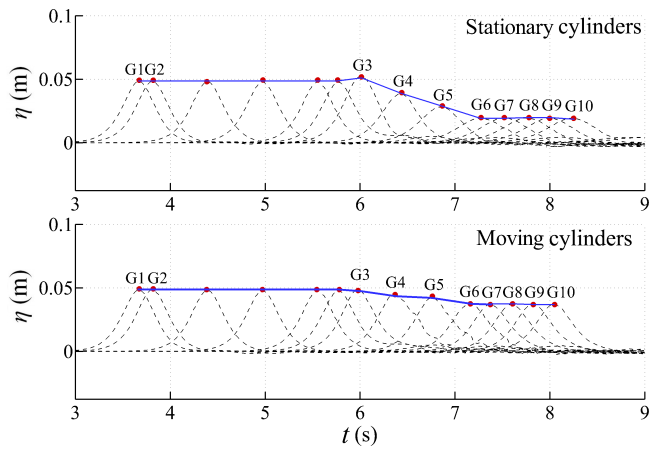


Figure 5. Wave surface evolutions for stationary and moving cylinders, $H_i = 0.05$ m.

2 Numerical model description

Among a number of open-source CFD codes available, IH-FOAM (Higuera et al., 2013, 2014) is specially designed for coastal engineering applications. IHFOAM was used by Maza et al. (2015) for direct numerical simulation of a solitary wave interacting with stationary vegetation. Alternatively, the model Flow-3D (Flow Science, Inc., 2012) is applied in this paper to conduct numerical simulations that include vegetation motion under wave action. Flow-3D provides exclusively the FAVOR (fractional area/volumes obstacle representation) technique (Hirt, 1993) and a general moving object (GMO) model that is capable of simulating the rigid body motion dynamically coupled with fluid flow. The FAVOR technique retains rectangular elements with a simple Cartesian grid system and has been shown to be one of the most efficient methods to treat immersed solid bodies (Xiao, 1999). The free water surface tracking in the model is accomplished by using the volume of fluid (VOF) method (Hirt and Nichols, 1981).

Referring to previous literature, the problem is idealized by a solitary wave passing on a group of emergent rigid cylinders. Considering the fluid to be incompressible, the continu-

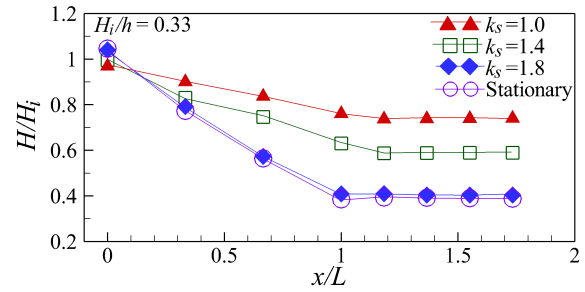


Figure 6. Comparison of wave height evolutions for moving cylinders with different spring constants.

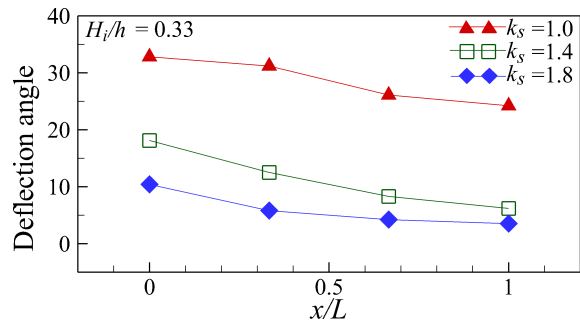


Figure 7. Comparison of the maximum deflection angle of moving cylinders with different spring constants.

ity and momentum equations for a moving object formulated with area and volume fraction functions are given as

$$\frac{\partial(u_i A_i)}{\partial x_i} = -\frac{\partial V_F}{\partial t}, \tag{1}$$

$$\frac{\partial u_i}{\partial t} + \frac{A_j u_j}{V_F} \frac{\partial u_i}{\partial x_j} = -\frac{1}{\rho} \frac{\partial p}{\partial x_i} + g_i + \frac{1}{\rho V_F} \frac{\partial}{\partial x_j} \left[2A_j [(\mu + \rho \nu_t) S_{ij} - \frac{2}{3} \rho k \delta_{ij}] \right], \tag{2}$$

where $S_{ij} = (\partial u_i / \partial x_j + \partial u_j / \partial x_i) / 2$, V_F is the fractional volume open to the flow and A_j is the fraction area for the subscript direction. The subscripts of i and $j = 1, 2, 3$ represent $x, y,$ and z directions. x_i and x_j represent Cartesian coordinates. u_i and u_j are the mean velocity component in subscript direction. t is the time, p is the pressure intensity, ρ is the fluid density, g_i is the gravitational acceleration, μ is the absolute viscosity, ν_t is the eddy viscosity, k is the turbulent kinetic energy, and δ_{ij} is the Kronecker delta function such that $\delta_{ij} = 1$ when $i = j$; $\delta_{ij} = 0$, when $i \neq j$.

The eddy viscosity ν_t in Eq. (2) takes the form as

$$\nu_t = c_\mu \frac{k^2}{\varepsilon}, \tag{3}$$

where k and ε represent the turbulent kinetic energy and turbulent energy dissipation rate, respectively, and c_μ is a constant. k and ε are related to the effect of space and time

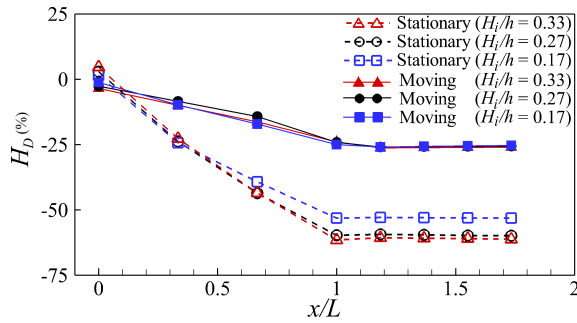


Figure 8. Comparison of wave height damping ratio between stationary and moving cylinders.

distribution of the turbulent motion, which can be solved by a variety of turbulent closure models such as a one-equation model, two-equation $k - \varepsilon$ model, renormalization group method (RNG $k - \varepsilon$ model), large eddy simulation (LES), and shear stress transport ($k - \omega$ SST) model. The RNG $k - \varepsilon$ turbulent model was originally derived by Yakhot and Orszag (1986) based on renormalization group methods and improved by Yakhot et al. (1992) with scale expansions for the Reynolds stress and production of dissipation terms. The RNG $k - \varepsilon$ model can be a useful turbulence model for practical engineering and scientific calculations (Speziale and Thangam, 1992). Choi et al. (2007) applied an RNG $k - \varepsilon$ turbulent model to the three-dimensional simulation of tsunami run-up around a conical island and demonstrated its computational efficiency and accuracy. The RNG $k - \varepsilon$ turbulent model has been proven to be reliable for a wider class of flows, and thus it is applied in this paper.

Referring to Yakhot et al. (1992), the turbulent transport equations of the RNG $k - \varepsilon$ model are expressed as

$$\frac{\partial k}{\partial t} + \frac{u_i A_i}{V_F} \frac{\partial k}{\partial x_i} = P - \varepsilon + \frac{1}{V_F} \frac{\partial}{\partial x_i} \left(\nu_t A_i \frac{\partial k}{\partial x_i} \right), \quad (4)$$

$$\frac{\partial \varepsilon}{\partial t} + \frac{u_i A_i}{V_F} \frac{\partial \varepsilon}{\partial x_i} = c_{\varepsilon 1} \frac{\varepsilon}{k} P - c_{\varepsilon 2} \frac{\varepsilon^2}{k} + \frac{1}{V_F} \frac{\partial}{\partial x_i} \left(\nu_t A_i \frac{\partial \varepsilon}{\partial x_i} \right), \quad (5)$$

where P is the turbulence kinetic energy production given by

$$P = 2\nu_t S_{ij} \hat{S}_{ij}, \quad \hat{S}_{ij} = \frac{1}{V_F} \left(A_j \frac{\partial u_i}{\partial x_j} + A_i \frac{\partial u_j}{\partial x_i} \right). \quad (6)$$

The coefficients are summarized as follows:

$$\begin{aligned} C_\mu &= 0.085, C_{\varepsilon 1} = 1.42 - \frac{\alpha(1 - \alpha/\alpha_o)}{1 + \beta\alpha^3} \\ C_{\varepsilon 2} &= 1.68, \sigma_k = 0.7179, \sigma_\varepsilon = 0.7179, \end{aligned} \quad (7)$$

where $\alpha = Sk/\varepsilon$, $S = (2S_{ij}\hat{S}_{ij})^{1/2}$, $\alpha_o = 4.38$, and $\beta = 0.015$.

For coupling the rigid body motion dynamically with fluid flow, the GMO model is adopted here. Compared with

the continuity equation for stationary obstacle problems, $-\partial V_F/\partial t$ in Eq. (1) is equivalent to an additional volume source term and exists only in mesh cells around the moving object boundary. It can be calculated using

$$-\frac{\partial V_F}{\partial t} = \frac{S_{\text{obj}}}{V_{\text{cell}}} u_{\text{obj}} n_j, \quad (8)$$

where V_{cell} is volume of a mesh cell; S_{obj} , n_j , and u_{obj} are, respectively, surface area, unit normal vector, and velocity of the moving object in the mesh cell. The relative transport equation for the VOF function F is given using

$$\frac{\partial F}{\partial t} + \frac{1}{V_F} \frac{\partial (F u_i A_i)}{\partial x_i} = -\frac{F}{V_F} \frac{\partial V_F}{\partial t}. \quad (9)$$

According to kinematics, general motion of a rigid body can be divided into a translational motion and a rotational motion. If the cylinder is considered to sway in the x direction with wave, angular velocity of the moving cylinder is the only non-zero component. Then the equations of motion of the cylinder are rendered as

$$T = J\dot{\omega}, \quad (10)$$

where T , J , and $\dot{\omega}$ are total torque, moment of inertia, and angular acceleration about the fixed axis. And the velocity of any point G on the moving cylinder is calculated by $V_G = \omega r_{G/C}$, where $r_{G/C}$ denotes distance from the fixed end C of the cylinder to point G .

In computing the coupling of fluid and rigid body interaction, the velocity and pressure of fluid flow are first solved. The hydrodynamics forces on the rigid body are then obtained and used to calculate the velocity of the rigid body. Then the volume and area fractions are updated according to the new position of the rigid body, and the source term can be calculated using Eq. (8). The flow field is computed repeatedly until the convergence is achieved. A similar GMO model has been applied for the numerical simulation of coupled motion of solid body and waves, e.g. in Bhinder et al. (2009), Dentale et al. (2014), and Zhao et al. (2014).

As for the boundary conditions for solving the governing equations of flow, the normal stress is in equilibrium with the atmospheric pressure while shearing stress is zero on the free surface. All of the solid surfaces were treated using the no-slip boundary condition. The variation of the turbulent energy and the turbulent energy dissipation on the free-surface boundary was set as zero in the normal direction. The solution of solitary wave derived from Boussinesq equations was employed as the incident wave.

3 Validation

Huang et al. (2011) conducted laboratory experiments in a wave flume for the solitary waves interacting with emergent rigid vegetation. The vegetation was represented by a

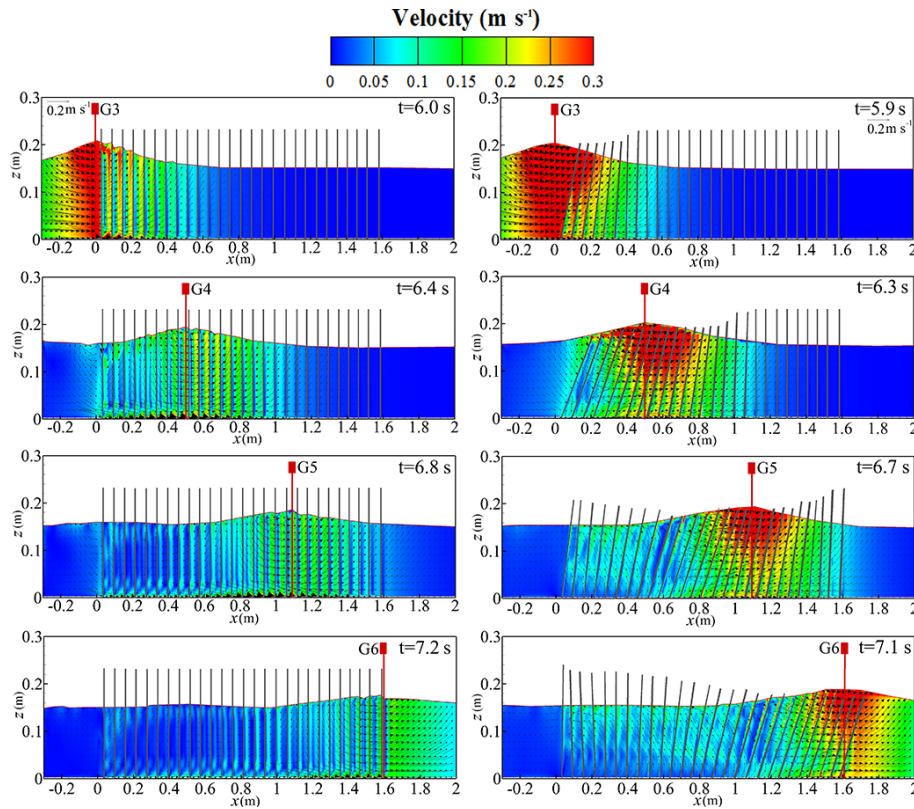


Figure 9. The snapshots of the velocity distribution for stationary cylinders (left) and moving cylinders (right), $H_i = 0.05$ m.

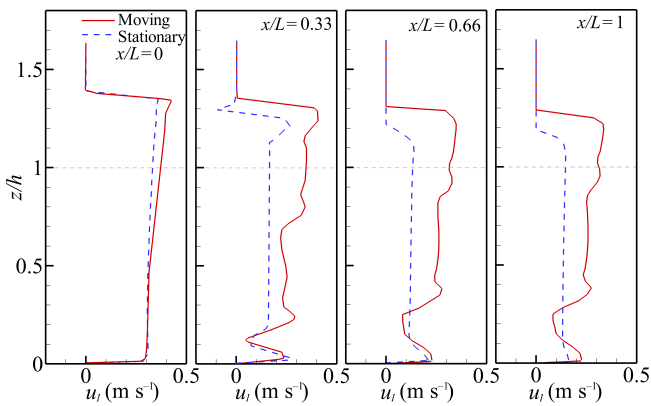


Figure 10. Comparison of the horizontal velocity profile for moving and stationary cylinders as wave crest passes each section, $H_i = 0.05$ m.

group of cylinders which were made of Perspex tubes with a uniform outer diameter of 0.01 m. The present computations used the same geometric configuration of Huang’s laboratory works. The water depth was uniform and equal to $h = 0.15$ m, and the cylinder height was 0.24 m. The arrangement of cylinders shown in Fig. 1 was selected to validate the present numerical simulation. Examples of two vegetation lengths, $L = 1.635$ and 0.545 m, are simulated here. The

numerical tank was set by 32 m long, 0.55 m wide, and 0.3 m height. Note that the verification of the model performance is only implemented by the case of stationary cylinders because the experimental information on the moving cylinders by solitary waves is unfortunately lacking.

Two different uniform computational meshes around the cylinder field, 0.002 and 0.001 m, respectively, were used to test the numerical accuracy and the sensitivity to grid size. Figure 2 shows that the FAVOR technique resolved successfully the geometry of cylinders using these two computational grids constructed. It indicates that FAVOR efficiently uses 29 and 17 points to define each cylinder for the mesh of 0.001 and 0.002 m, respectively.

Figure 3 shows the comparison of free-surface evolution between the present numerical results and experimental measurements for an incident wave height $H_i = 0.05$ m considering the vegetation length $L = 1.635$ m. The results obtained by the direct simulation using IHFOAM with $k - \omega$ SST turbulent model in Maza et al. (2015) were also shown in the figure. The comparisons show that the present numerical results are in good agreement with both the laboratory experiments and previous numerical simulations. The second validation is performed by considering the vegetation length $L = 0.545$ m to compare with Fig. 14 of Maza et al. (2015) using $H_i = 0.05$ m. The simulated result of wave height evolution along the vegetation shown in Fig. 4 depicts

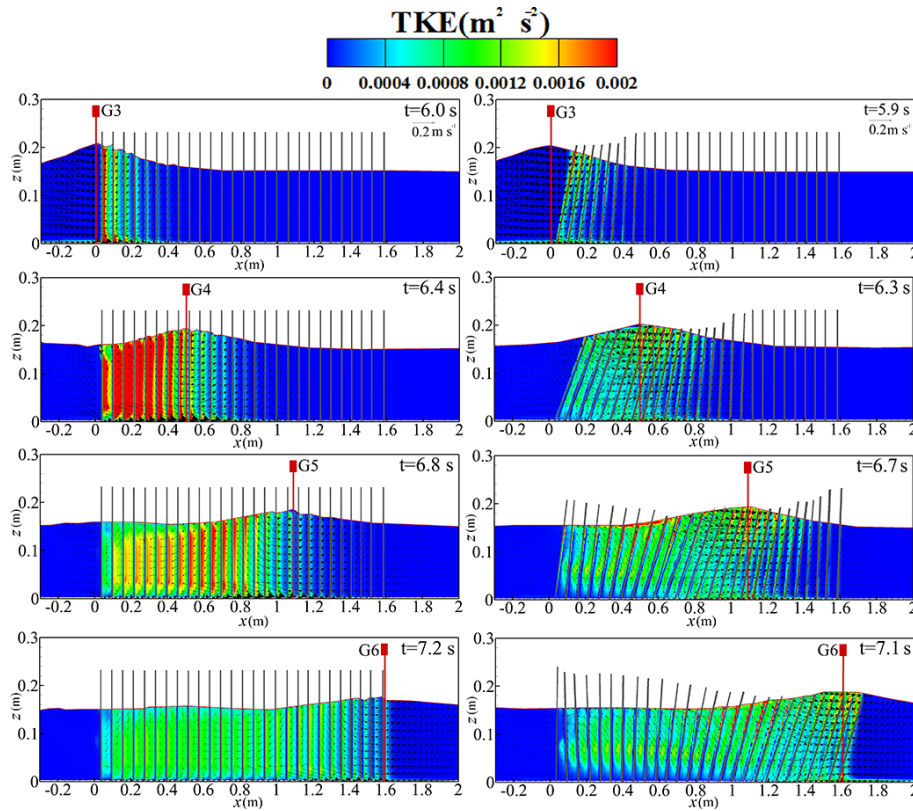


Figure 11. Snapshots of TKE for stationary cylinders (left) and moving cylinders (right), $H_i = 0.05$ m.

a good agreement with previous numerical results, though the present simulation used a different turbulent model. The comparisons shown in Figs. 3 and 4 also validate that there are almost no differences in the free-surface or wave height evolution for the two computational meshes.

4 Results and discussion

The above comparisons demonstrated that the present numerical model is capable of simulating accurately the wave evolution by the group cylinders. The following simulations are performed for a solitary wave passing through both the stationary and moving cylinders. The characteristics of the surface elevation evolution, the flow field variation, and the turbulent kinetic energy (TKE) are analysed and compared between stationary and moving cylinders. The numerical domain and the arrangement of cylinders used in the following simulations are the same as in previous section. The uniform fine mesh with 0.001 m is used for the following computations.

The moving cylinders induced by waves are set up by the GMO model for coupling the cylinder's motion and fluid flow dynamically. Similar to Kazemi et al. (2015), each cylinder end was simplified by attaching a torsion spring connector on the bottom in the model. The use of torsion

spring could not completely reproduce the natural bending behaviour of the mangrove tree, but it allows the cylinders to move with the passing wave. Peltola et al. (2000) and Husrin (2013) indicated that the deflection angles for a broken trunk may range from 23 to 42°. In the numerical tank with small model scale, too high a value of the specific gravity and lower spring constant will produce too large a deflection angle of the cylinders under wave action. Therefore, after many numerical tests, the spring constants are set to values of $k_s = 1\text{--}1.8$ kgw m⁻¹ with the cylinder's specific gravity of 0.25 to affirm that cylinders can return back to their original position after being hit by waves.

4.1 Free-surface evolution

The numerical free-surface evolutions along the stationary and moving cylinders, respectively, are shown in Fig. 5. The spring constant is set by $k_s = 1.0$ kgw m⁻¹ in this case. It can be seen that the free-surface elevation decays rapidly along the stationary cylinders but decays mildly along the moving cylinders.

Figure 6 shows the comparison of wave height evolution for moving cylinders with different spring constants, which can be seen that the results of moving and stationary cylinders are almost identical as $k_s = 1.8$ kgw m⁻¹. The smaller spring constant obtains smaller wave height damping. In ad-

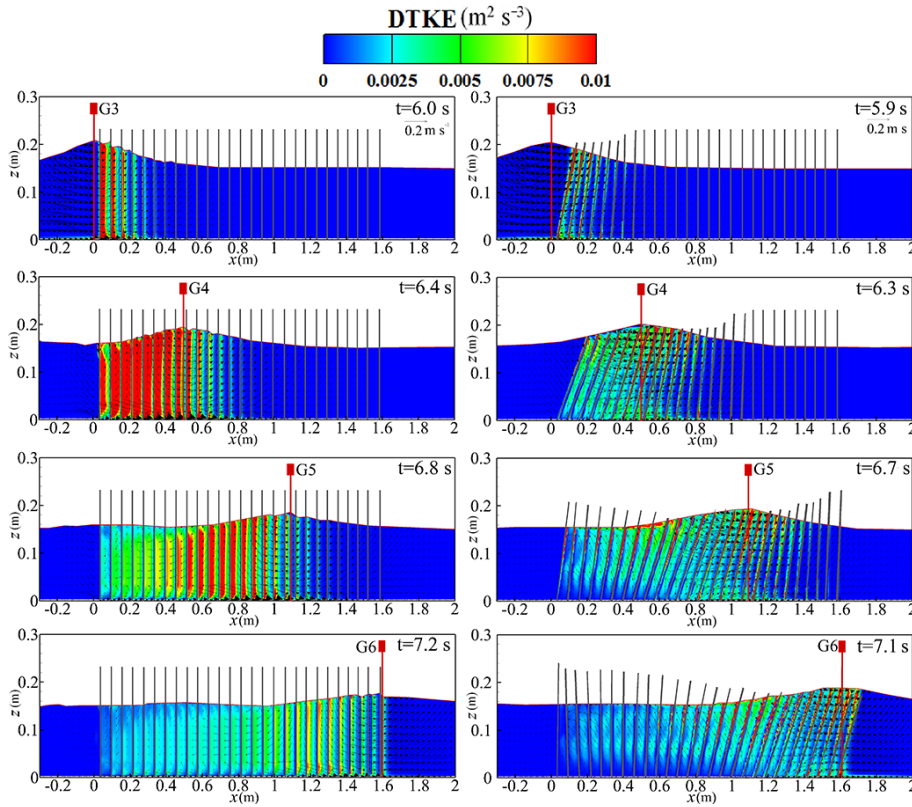


Figure 12. Snapshots of DTKE for stationary cylinders (left) and moving cylinders (right), $H_i = 0.05$ m.

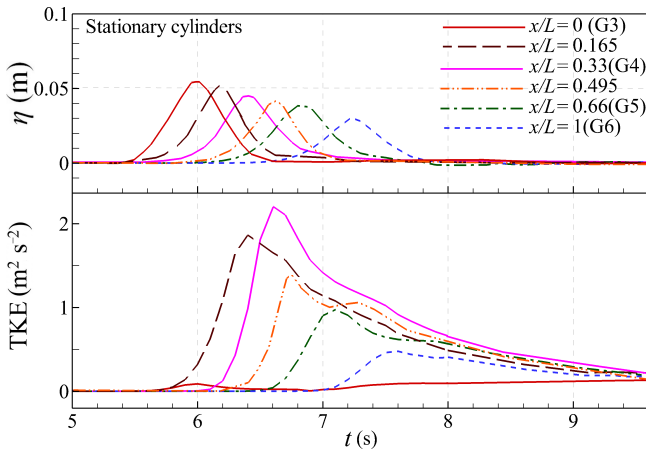


Figure 13. The time evolution of surface elevation and TKE at each section for stationary cylinders, $H_i = 0.05$ m.

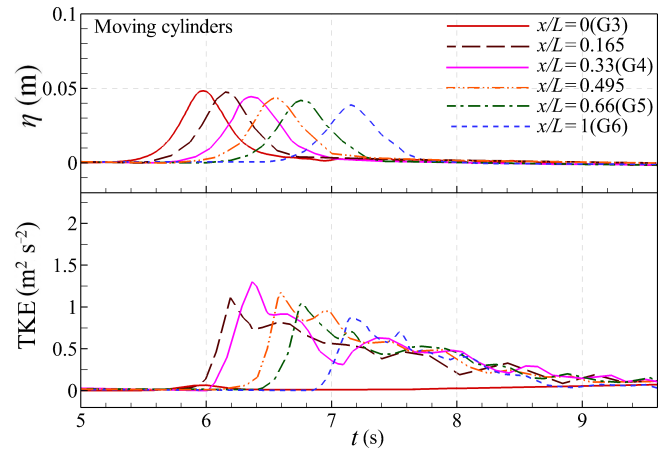


Figure 14. The time evolution of surface elevation and TKE at each section for moving cylinders, $H_i = 0.05$ m.

dition, Fig. 7 shows that the smaller spring constant produces the larger deflection of cylinder. It also shows that the deflection decreases along the cylinders. It is noted that the spring constant $k_s = 1.0 \text{ kgw m}^{-1}$ is used in the following examples.

Figure 8 shows the variation of the wave height damping ratio, $H_D = (H - H_i)/H_i$, along the cylinder array for different incident wave heights. It can be seen that the maxi-

imum wave height damping ratio for $H_i/H = 0.33$ is approximately 26 % for the moving cylinders but could reach 61 % for the stationary cylinders. The results show that the wave height damping of the stationary cylinders is working better than by the moving cylinders. That is, the wave height decay can be overestimated if the coastal vegetation was considered as a stationary state.

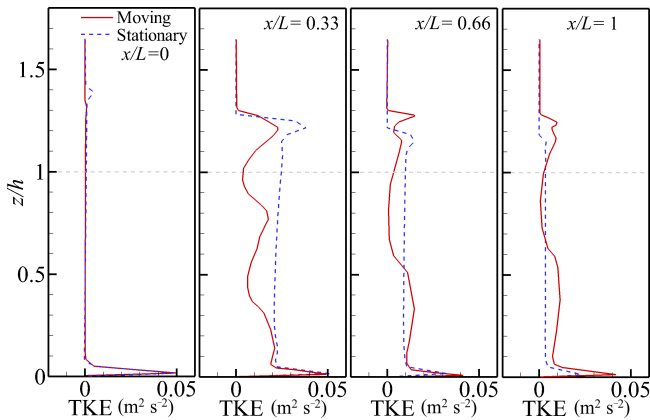


Figure 15. Comparison of vertical profiles of TKE as wave crest passes through each section, $H_i = 0.05$ m.

4.2 Flow field evolution

Figure 9 shows the snapshots of velocity distribution at the centre line of the tank for moving and stationary cylinders as the solitary wave crest passes through gauges G3 to G6 for an incident wave height $H_i = 0.05$ m. It can be observed that the water velocity reduces rapidly along the array of stationary cylinders. However, the flow velocity under the wave crest is not markedly damped along the moving cylinders because they have angular motion by wave action and even become immersed in the water. Figure 10 shows a comparison of the horizontal velocity profile as a wave crest passes through gauges G3 to G6, i.e. $x/L = 0, 0.33, 0.66,$ and 1.0 , for moving and stationary cylinders. It can be seen that the velocity profiles have multiple shear layers due to the motion effect of cylinders.

4.3 Turbulent kinetic energy evolution

The TKE will be generated and will dissipate during the wave when interacting with the group of cylinders. The turbulent kinetic energy (k) and the turbulent kinetic energy dissipation rate (DTKE) (ε) are obtained from the RNG $k - \varepsilon$ turbulent closure model while the general RANS equations is solving. We focus on when and where the maximum TKE occurs for an incident wave height $H_i = 0.05$ m.

Figures 11 and 12 display the snapshots of the spatial distribution of the TKE and the DTKE for stationary and moving cylinders, respectively, when the wave crest passes through gauges G3 to G6. It shows that the turbulent kinetic energy starts generating and dissipating after the wave crest impinges on the front row of cylinders. It can be seen that the characteristics of spatial distribution of TKE and DTKE for moving cylinders or stationary cylinders are very similar. Figures 13 and 14 display the time variations of TKE at each section ($x/L = 0-1$), which shows that the maximum TKE occurs at $x/L = 0.33$ of both cylinders. The result is that the maximum TKE does not occur when the wave crest reaches

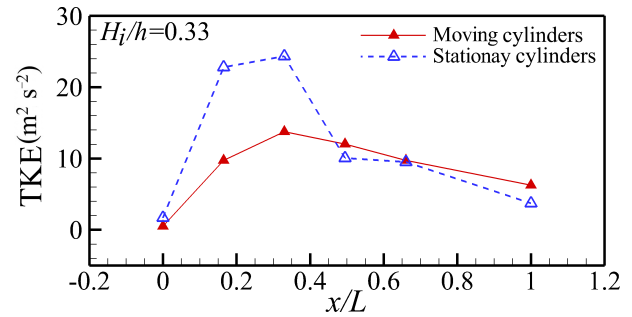


Figure 16. Comparison of total TKE evolution along cylinder array, $H_i = 0.05$ m.

the cylinders ($x/L = 0$). This result is similar to Maza et al. (2015), who found that the maximum turbulent intensity does not develop when the wave crest reaches the cylinders.

Figure 13 also shows that there is a time lag between the occurrence of maximum TKE and the maximum wave elevation for stationary cylinders, but there is almost no lag for moving cylinders. That is, the maximum TKE is produced after the wave crest passes each section for the case of stationary cylinders. However, for moving cylinders, the maximum TKE occurs at the wave crest when passing each section. It can also be seen in Fig. 14 that multiple peaks of the TKE evolution exist in the case of moving cylinders during the return to its original position, and the peak values decrease with time to zero.

Figure 15 shows the comparisons of vertical profiles of TKE between moving and stationary cylinders as the wave crest passes through gauges G3 to G6. It confirms that almost no TKE is produced at $x/L = 0$. Like the horizontal velocity profiles, it can be seen that multiple shear layers exist in the vertical profile of TKE due to the moving effect of cylinders. Figure 16 is the comparison of total TKE evolution along the array of both cylinders, in which the total TKE is calculated by the integral of time evolution shown in Figs. 13 and 14. This figure shows that the largest TKE occurs at $x/L = 0.33$ for both cylinders. The maximum TKE produced by the interaction of wave and moving cylinders is clearly less than by the stationary cylinders.

5 Conclusions

A numerical simulation based on the three-dimensional RANS equations and RNG $k - \varepsilon$ turbulent model was implemented to investigate the moving effect of coastal vegetation on the damping of tsunami wave by means of solitary waves passing over a group of emergent rigid cylinders. The FAVOR technique and GMO model were employed in this paper for simulating the coupling of fluid and rigid body interaction. The present numerical model was first validated using both previous laboratory data and numerical results of surface elevation evolution along the stationary cylinders.

Then the evolutions of wave height, flow field, and turbulent kinetic energy along both stationary and moving cylinders were investigated. The simulated results showed that the wave height damping by the moving cylinders is much less than by the stationary cylinders. The maximum turbulent kinetic energy produced by the interaction of wave and moving cylinders was also clearly less than by the stationary cylinders. That implies that the tsunami damping by the coastal vegetation can be overestimated if the moving effect of vegetation is not considered.

Data availability. The data used for the validation were cited from Huang et al. (2011) and Maza et al. (2015). To access the numerical dataset, please contact the corresponding author.

Competing interests. The authors declare that they have no conflict of interest.

Acknowledgements. The authors would like to express their appreciation to Maria Maza, University of Cantabria, Spain, and the anonymous reviewer for their valuable comments and suggestions.

Edited by: M. Gonzalez

Reviewed by: M. Maza and one anonymous referee

References

- Anderson, M. E., Smith, J. M., and McKay, S. K.: Wave dissipation by vegetation, Coastal and Hydraulics Engineering Technical Note ERDC/CHL CHETN-I-82, US Army Engineer Research and Development Center, Vicksburg, MS, 2011.
- Augustin, L. N., Irish, J. L., and Lynett, P.: Laboratory and numerical studies of wave damping by emergent and near-emergent wetland vegetation, *Coast. Eng.*, 56, 332–340, doi:10.1016/j.coastaleng.2008.09.004, 2009.
- Baird, A.: False hopes and natural disasters, *New York Times*, 26 December 2006.
- Bhinder, M. A., Mingham, C. G., Causon, D. M., Rahmati, M. T., Aggidis, G. A., and Chaplin, R. V.: A joint numerical and experimental study of a surging point absorbing wave energy of converter (WRASPA), *Proc. ASME 28th Inter. Conf. Ocean, Offshore and Arctic Eng., OMAE2009-79392*, doi:10.1115/OMAE2009-79392, 31 May–5 June 2009.
- Choi, B. H., Kim, D. C., Pelinovsky, E., and Woo, S. B.: Three dimensional simulation of tsunami runup around conical island, *Coast. Eng.*, 54, 618–629, doi:10.1016/j.coastaleng.2007.02.001, 2007.
- Cochard, R., Ranamukhaarachchi, S. L., Shivakoti, G. P., Shipin, O. V., Edwards, P. J., and Seeland, K. T.: The 2004 tsunami in Aceh and Southern Thailand: A review on coastal ecosystems, wave hazards and vulnerability, *Perspectives in Plant Ecology, Evolution and Systematics* 10, 3–40, doi:10.1016/j.ppees.2007.11.001, 2008.
- Danielsen, F., Sorensen, M. K., Olwig, M. F., Selvam, V., Parish, F., Burgess, N. D., Hiraishi, T., Karunagaran, V. M., Rasmussen, M. S., Hansen, L. B., Quarto, A., and Suryadiputra, N.: The Asian tsunami: a protective role for coastal vegetation, *Science*, 310, p. 643, doi:10.1126/science.1118387, 2005.
- Dentale, F., Donnarumma, G., and Pugliese Carratelli, E.: Simulation of flow within armour blocks in a breakwater, *J. Coast. Res.*, 30, 528–536, doi:10.2112/JCOASTRES-D-13-00035.1, 2014.
- Flow Science, Inc.: *Flow-3D User's Manuals*, Santa Fe, NM, 2012.
- Harada, K. and Kawata, Y.: Study on the effect of coastal forest to tsunami reduction, *Annals of Disas. Prev. Res. Inst., Kyoto Univ.*, No. 47 C, 2004.
- Higuera, P., Lara, J. L., and Losada, I. J.: Realistic wave generation and active wave absorption for Navier–Stokes models: application to OpenFOAM, *Coast. Eng.*, 71, 102–118, doi:10.1016/j.coastaleng.2012.07.002, 2013.
- Higuera, P., Lara, J. L., and Losada, I. J.: Three-dimensional interaction of waves and porous coastal structures using OpenFOAM. Part I: formulation and validation, *Coast. Eng.*, 83, 243–258, 2014.
- Hiraishi, T. and Harada, K.: Greenbelt tsunami prevention in south-Pacific region, Report of the Port and Airport Research Institute, 42, 3–25, 2003.
- Hirt, C. W. and Nichols, B. D.: Volume of fluid (VOF) method for dynamics of free boundaries, *J. Comp. Phys.*, 39, 201–225, doi:10.1016/0021-9991(81)90145-5, 1981.
- Hirt, C. W.: Volume-fraction techniques: powerful tools for wind engineering, *J. Wind Eng. Indust. Aerodynamics*, 46–47, 327–338, doi:10.1016/0167-6105(93)90298-3, 1993.
- Huang, Z., Yao, Y., Sim, S. Y., and Yao, Y.: Interaction of solitary waves with emergent stationary vegetation, *Ocean Eng.*, 38, 1080–1088, doi:10.1016/j.oceaneng.2011.03.003, 2011.
- Husrin, S.: Attenuation of solitary waves and wave trains by coastal forests, Doctoral Thesis, TU Braunschweig, Germany, 2013.
- Husrin, S. and Oumeraci, H.: A new tree parameterization approach for modelling tsunami attenuation by coastal forests, *Proc. 7th Inter. Conf. Asian and Pacific Coasts*, Bali, Indonesia, 24–26 September 2013.
- Husrin, S., Strusińska, A., and Oumeraci, H.: Experimental study on tsunami attenuation by mangrove forest, *Earth, Planets Space*, 64, 973–989, doi:10.5047/eps.2011.11.008, 2012.
- Iverson, L. R. and Prasad, A. M.: Using landscape analysis to assess and model tsunami damage in Aceh province, Sumatra, *Landscape Ecol.*, 22, 323–331, doi:10.1007/s10980-006-9062-6, 2007.
- Kazemi, A., Parry, S., van de Riet, K., and Curet, O.: The effect of porosity and flexibility on the hydrodynamics behind a mangrove-like root model, *APS Division of Fluid Dynamics (Fall) 2015*, abstract #A25.007, 2015.
- Maza, M., Lara, J. L., and Losada, I. J.: Tsunami wave interaction with mangrove forests: a 3-D numerical approach, *Coast. Eng.*, 98, 33–54, doi:10.1016/j.coastaleng.2015.01.002, 2015.
- Peltola, H., Kellomäki, S., Hassinen, A., and Granander, M.: “Mechanical stability of Scots pine, Norway spruce and birch: an analysis of tree-pulling experiments in Finland”, *Forest Ecol. Manag.*, 135, 143–153, doi:10.1016/S0378-1127(00)00306-6, 2000.
- Shuto, N.: The effectiveness and limit of tsunami control forests, *Coastal Engineering in Japan*, 30, 143–153, 1987.

- Speziale, C. G. and Thangam, S.: Analysis of an RNG based turbulence model for separated flows, *Int. J. Eng. Sci.*, 30, 1379–1388, doi:10.1016/0020-7225(92)90148-A, 1992.
- Strusińska-Correia, A., Husrin, S., and Oumeraci, H.: Tsunami damping by mangrove forest: a laboratory study using parameterized trees, *Nat. Hazards Earth Syst. Sci.*, 13, 483–503, doi:10.5194/nhess-13-483-2013, 2013.
- Strusińska, A., Husrin, S., and Oumeraci, H.: Attenuation of solitary wave by parameterized flexible mangrove model, *Proc. 34th Intl. Conf. Coast. Eng.*, doi:10.9753/icce.v34.management.13, 2014.
- Teh, S. Y., Koh, H. L., Liu, P. L. F., Ismail, A. I. M., and Lee, H. L.: Analytical and numerical simulation of tsunami mitigation by mangroves in Penang, Malaysia, *J. Asian Earth Sci.*, 36, 38–46, doi:10.1016/j.jseas.2008.09.007, 2009.
- Wolanski, E.: Synthesis of the protective functions of coastal forests and trees against natural hazards, *Proceedings of the regional technical workshop on Coastal protection in the aftermath of the Indian Ocean tsunami: What role for forests and trees?*, Food and Agriculture Organization of the United Nations, 2006.
- Wu, W. C., Ma, G., and Cox, D. T.: Modeling wave attenuation induced by the vertical density variations of vegetation, *Coast. Eng.*, 112, 17–27, doi:10.1016/j.coastaleng.2016.02.004, 2016.
- Xiao, F.: A computational model for suspended large rigid bodies in 3D unsteady viscous flows, *J. Comput. Phys.*, 155, 348–379, doi:10.1006/jcph.1999.6340, 1999.
- Yakhot, V. and Orszag, S. A.: Renormalization group analysis of turbulence, I. Basic theory, *J. Sci. Comput.*, 1, 3–51, doi:10.1007/BF01061452, 1986.
- Yakhot, V., Orszag, S. A., Thangam, S., Gatski, T. B., and Speziale, C. G.: Development of turbulence models for shear flows by a double expansion technique, *Phys. Fluids A*, 4, 1510–1520, doi:10.1063/1.858424, 1992.
- Yanagisawa, H., Koshimura, S., Goto, K., Miyagi, T., Imamura, F., Ruangrassamee, A., and Tanavud, C.: The reduction effects of mangrove forest on a tsunami based on field surveys at Pakarang Cape, Thailand and numerical analysis, *Estuarine, Coastal and Shelf Science*, 81, 27–37, doi:10.1016/j.ecss.2008.10.001, 2009.
- Zhang, X., Chua, V. P., and Cheong, H. F.: Hydrodynamics in mangrove prop roots and their physical properties, *Journal of Hydro-environment Research*, 9, 281–294, doi:10.1016/j.jher.2014.07.010, 2015.
- Zhao, X., Ye, Z., Fu, Y., and Cao, F.: A CIP-based numerical simulation of freak wave impact on a floating body, *Ocean Eng.*, 87, 50–63, doi:10.1016/j.oceaneng.2014.05.009, 2014.